3

Fluorination of Graphitic Nanocarbons for Supercapacitors

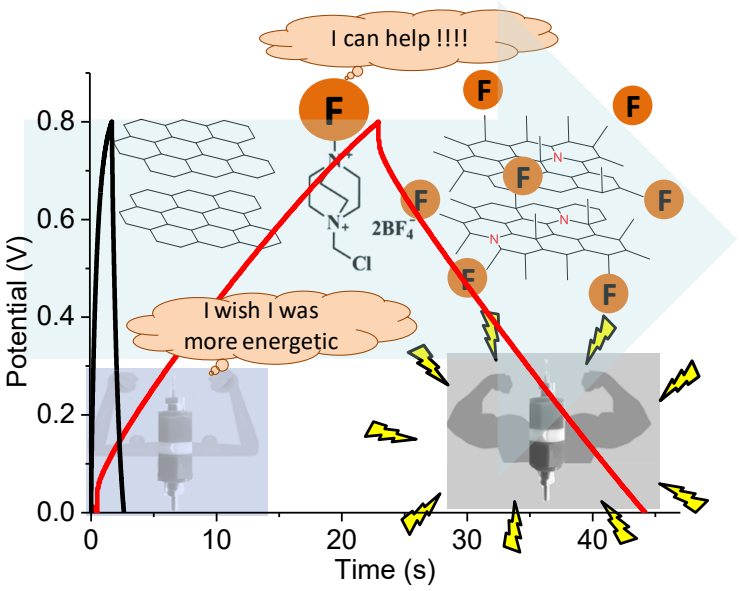

3.1 Introduction

Fluorinated graphene is one of the most important fluorocarbons and has become a rising star of graphene derivatives because of its high chemical stability, good thermal stability (400 °C), high theoretical specific capacity, improved optical and electron transfer properties from its parent graphene because of the formation of polar C-F bond which has high bond energy. It has also been found to be stable in liquids such as water, acetone, and propanol under ambient conditions [Nair et al., 2010]. In fluorinated graphene, different F/C ratio is used to tailor the electronic conductivity since it enables the transition from metallic/semiconducting to an insulating nature [Wang et al., 2012]. The fluorinated graphene with a low F/C ratio shows semiconducting behavior because of sp^2 hybridized carbon network, whereas with a high F/C ratio, the π-conjugated network is destroyed and act as an insulating behavior. This increase in bandgap is because of the interaction between the p-orbital of F and the π-orbital of C. Thus, the C-F structural characteristics offer a strategy to control the properties of fluorocarbons. An *et al.* synthesized fluorinated graphene hydrogels with semi-ionic bonds using HF in the hydrothermal process and obtained high specific capacitance of 227 F/g with enhanced rate capabilities [An et al., 2016]. In a similar study by the hydrothermal method, Peng *et al.* fabricated fluorinated graphene with semi-ionic C-F bonds and hybridized it with CoAl-layered double hydroxide and reported high capacitance of 1222 F/g, enhanced rate capability, and stable capacitance retention [Peng et al., 2017]. Jung *et al.* synthesized surface-fluorinated MWCNT using fluorine gas which exhibited a specific capacitance two times higher than that of the pristine counterpart due to surface polarity induced by the fluorine functional group [Jung et al., 2015].

Commercially available carbon materials with high specific surface area and low cost can serve as an ideal material for supercapacitor application provided its intrinsic electrical conductivity and wettability is improved by surface modification [Lee, 2007]. Several efforts have been made in this direction to improve the electrochemical supercapacitive performance of carbon by fluorination route. For example, Kim *et al.* fluorinated activated carbon using HF for enhanced kinetics in supercapacitor applications, which is attributed to the semi-ionic bonding character

between fluorine and activated carbon [Kim et al., 2014]. Lee *et al.* reported 15.8-47.3% increase in specific capacitance of fluorinated activated carbon nanofibres despite a significant decrease in specific surface area and pore volume upon fluorination [Jeong et al., 2013]. Lee *et al.* introduced fluorine in carbon matrix using F_2 gas for high capacitance values (491 F/g). The enhancement in supercapacitive behavior, in this case, was attributed to the synergistic effect of increased polarisation, increment in pore volume and surface area due to fluorination [Jung et al., 2011].

3.1.1 Objectives of Work

The objectives of this work are as follows:

1. To perform fluorination of commercially available low quality carbon material at milder conditions via solution-processable method using F-TEDA as a source of fluorine.
2. To study the effect of fluorination on the electrochemical charge storage of fluorinated carbon materials for EDLCs.

3.2 Experimental

3.2.1 Fluorination of Graphitic Carbon

Carbon Black (Vulcan Carbon XC-72R) was purchased from Gautam Dyes & Chemicals Inc. India. For fluorination, 100 mg Vulcan Carbon (VC) was treated with F-TEDA (Selectfluor™, 1-chloromethyl-4-fluorodiazoniabicyclo [2.2.2] octane bis(-tetrafluoroborate)) (2.82 mM in water) for 3 h at 70 ^{o}C with continuous stirring. The processed VC powder was obtained via vacuum filtration using 0.45 µm pore size PTFE filter paper. Further, it was heated at 150 ^{o}C in a hot air oven to obtain fluorinated Vulcan Carbon (F-VC).

3.2.2 Device Fabrication

Carbon Cloth (CC) with resistance of 2 Ω/sq was purchased from Fuel Cell Earth LLC and used after cleaning with isopropyl alcohol solvent without any surface modification. A paste of VC and F-VC (10 mg) was prepared using 80 µL of Nafion (CAS: 31175-20-9, Sigma Aldrich) in 750 µL of IPA. The paste was then drop coated on pre-cut carbon cloth of 5 mm diameter and left for air-drying overnight (25 ^{o}C). Finally, symmetric two-electrode supercapacitor assembly was fabricated in Swagelok cell using VC loaded carbon cloth electrodes and 10 mm diameter separator (Celgard™, 25 µm thick) in ambient conditions.

3.2.3 Material Characterization

Surface composition and chemical states of pristine and fluorinated VC samples were analyzed with an Omicron Nanotechnology (Oxford instruments) X-ray photoelectron spectroscopy (XPS) instrument equipped with monochromatic Al Kα radiation. The elemental composition was calculated using CasaXPS. Raman analysis was performed using Renishaw instruments with 785 nm laser excitation. Raman and XPS data were fitted using Fityk 1.3.1 software. BET specific surface area was analyzed by N_2 adsorption–desorption isotherms (Quntachrome autosorb iQ3). Contact angle was measured on Contact Angle Meter DMe-211Plus.

3.2.4 Electrochemical Measurements

The electrochemical measurements in three-electrode geometry were performed in a 3 M KOH solution using Ag/AgCl as a reference electrode and platinum wire as a counter electrode. The Ag/AgCl electrode was refilled with a saturated KCl solution and calibrated for every electrode measurement to ensure the correctness in the results. The working electrode was prepared on a

glassy carbon electrode by drop-casting 5 µL dispersion of the carbon material (10 mg) in 750 µL isopropyl alcohol and 80 µL Nafion (CAS: 31175-20-9, Sigma Aldrich). Electrochemical measurements were performed on CH-660 electrochemical workstation. Cyclic Voltammetry curves were acquired in the potential range between 0–0.8V at different scan rates from 10–100 mV/s. Specific capacitance from Cyclic Voltametry (CV) plots was calculated using the formula $C=\frac{\int IdV}{2m\times s\times \Delta V}$ where $\int IdV$ is the area under the I-V curve, m is the mass of VC loaded on carbon cloth; s is the scan rate and ΔV is the voltage window. Galvanostatic charge-discharge (GCD) measurements were carried out at current densities ranging from 0.05–0.5 A/g. Specific capacitance of the cell was calculated from GCD curves using formula, $C=\frac{2i\,\Delta t}{m\,\Delta V}$ where i is the current density, Δt is the discharge time, m is the mass of VC loaded on carbon cloth and ΔV is the potential range of the charge-discharge cycle. Energy density and power density were calculated using the formula $E=\frac{1}{8}\times C\times \Delta V^2$ and $P=\frac{E}{\Delta t}$ where E is the energy density, C is the specific capacitance, ΔV is the voltage window, P is the power density and Δt is the discharge time. Electrochemical impedance analysis of the devices was performed in 0.1–10^6 Hz frequency range.

3.3 Result and Discussion

3.3.1 Fluorination of Vulcan Carbon

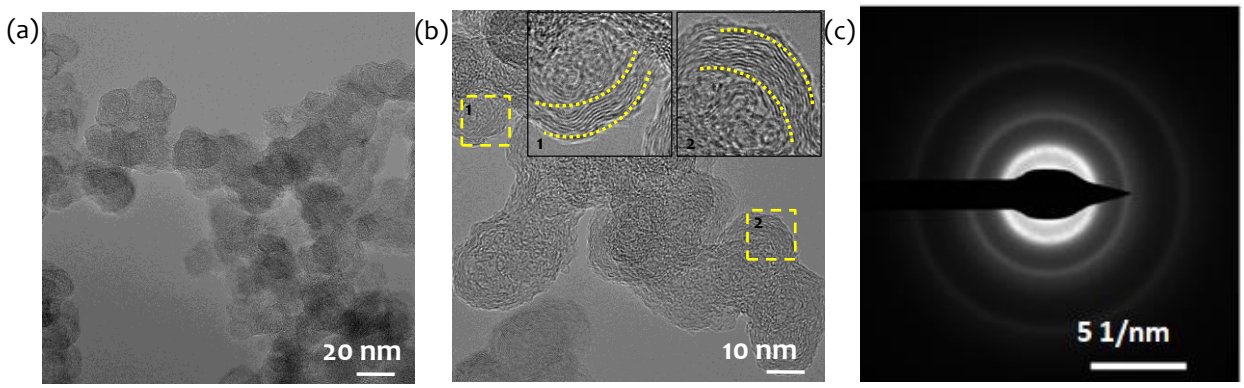

Figure 3.1: (a) TEM and (b) HRTEM images of VC. Insets in b show the magnified view. (c) Electron diffraction pattern of VC.

VC consists of carbon black powder with particle size of ~20 nm (Figure 3.1a). The HRTEM image in Figure 3.1b shows that the carbon particles comprise of graphitic shell concentrically oriented around amorphous core (inset, Figure 3.1b). Graphitic layers, with an interplanar distance of ~0.35 nm, extend laterally up to 3-4 nm (Figure 3.1b). Electron diffraction pattern shows that VC is dominantly amorphous in nature despite of a visible crystalline graphitic shell in HRTEM image (Figure 3.1c). In comparison to the non-graphitic activated carbon, carbon black is an easily available source of carbon with graphitic constituents that imparts it higher conductivity. VC with surface area of 248 m^2/g is neither microporous nor mesoporous and possesses lowest surface area among all forms of carbon (shown later in figure 3.2b,c). However, it is available as a bulk source of carbon [Pérez-Rodríguez et al., 2018] and thus used for improvising its properties by fluorination process developed in this study.

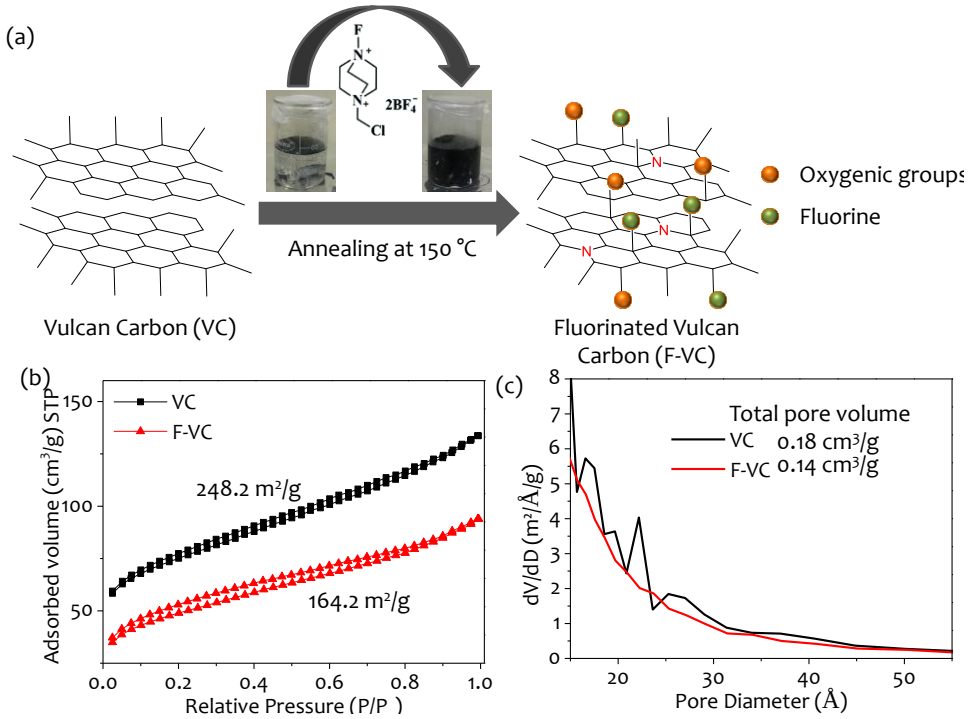

Figure 3.2: (a) Schematic demonstrating the steps involved in the fluorination of VC using F-TEDA as a precursor. (b) N_2 adsorption-desorption BET isotherm of VC and F-VC. (c) Pore size distribution of VC and F-VC carbon material.

The fluorination of VC is performed following the method as demonstrated by the schematic in Figure 3.2a. The VC is functionalized with F-TEDA precursor by stirring in aqueous solution at optimized heating conditions of 70 °C for 3 h. The wettability of carbon in F-TEDA solution results in a uniform dispersion and is clearly an indication of physical adsorption of molecules on the carbon that reduces the hydrophobicity. Thereafter, the functionalized carbon is filtered and heated to 150 °C to form reactive fluorine species that probably bond with the surface of VC resulting in the formation of fluorinated Vulcan Carbon (F-VC). The surface area and pore volume of VC decrease significantly on fluorination due to the formation of functional groups as reported in the literature as well (Figure 3.2b,c) [Jung et al., 2009].

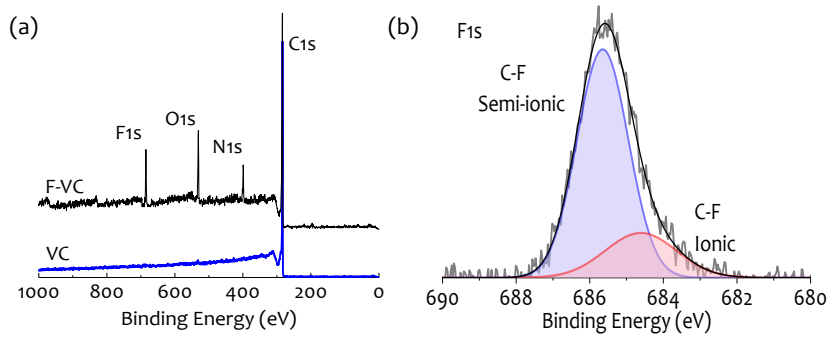

Figure 3.3: (a) Survey scan of F-VC and VC. (b) High resolution deconvoluted F1s spectra of F-VC.

X-ray Photoelectron Spectroscopy (XPS) characterization of F-VC and VC is performed to determine the nature and extent of covalent functionalization of graphitic carbon. The measurements were performed after rinsing the samples gently with water post-preparation to remove the excess of unreacted and physisorbed F-TEDA molecules. The complete range survey spectra of F-VC and VC are shown in Figure 3.3a. In the XPS survey spectrum of F-VC, peaks of F1s, N1s and O1s are additionally observed in contrast to the pristine VC. In deconvoluted F1s high resolution spectra, two peaks at 684.6 eV and 685.6 eV are assigned to ionic C-F and semi-ionic C-F bond respectively in which the original sp^2 hybridization of the carbon atoms are retained (Figure 3.3b) [Jiang et al., 2015; Peera et al., 2016]. The integrated areas under the peaks results in fluorine content of 10.2 at% where 8.02 at% corresponds to the fluorine atoms having

semi-ionic C-F bond and 2.17 at% to the ionic C-F bond. The emergence of the C-F bond in C1s and F1s verifies that fluorine atoms are functionalized in the VC matrix successfully [An et al., 2016].

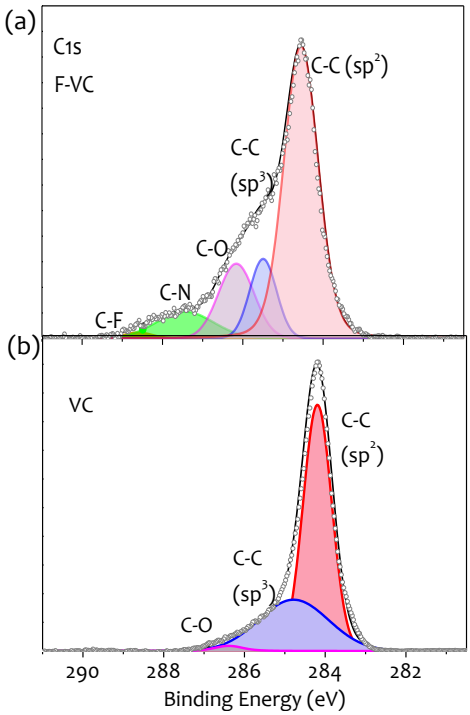

Figure 3.4: High resolution deconvoluted C1s spectra of (a) F-VC and (b) VC.

Figure 3.4a shows the high-resolution deconvoluted C1s spectra of F-VC. C1s peak is deconvoluted into five peaks centered at 284.5 eV (C=C), 285.4 eV (C-C), 286.2 eV (C-O), 287.4 eV (C-N) and 288.6 eV (semi-ionic C-F). The peak positions are identified from the literature reports tabulated in Table 3.1. The peak at 288.6 eV confirms the presence of semi-ionic C-F bonds [Huang et al., 2015]. This may also be compared with pristine VC (Figure 3.4b) which has only three peaks centered at 284.2, 284.8 and 286.4 eV corresponding to C-C, C=C and C-O respectively.

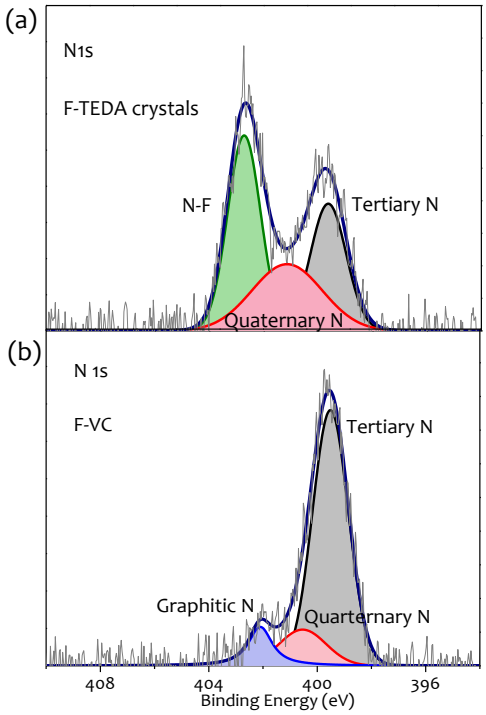

Figure 3.5: High resolution deconvoluted N1s spectra of (a) F-TEDA crystals and (b) F-VC.

To understand the nature of nitrogen signals present in XPS data, high-resolution deconvoluted N1s spectra of F-VC is compared with that of pristine F-TEDA crystals (Figure 3.5a). The N1s spectrum of pristine F-TEDA solid crystals is deconvoluted into 3 peaks centered at 399.6, 401.1 and 402.7 eV respectively associated with tertiary nitrogen, quaternary nitrogen and fluorine bonded nitrogen (N-F) (Table 3.1). Two peaks corresponding to the quaternary nitrogen and fluorine bonded nitrogen are structurally expected whereas tertiary nitrogen in F-TEDA originate from the removal of fluorine as an electrophile from the molecule. The N1s spectrum of F-VC is also deconvoluted into three peaks (Figure 3.5b). The peaks centered at 399.5 eV and 400.5 eV corresponding to the tertiary and quaternary nitrogen matches with that of F-TEDA moiety. Further, absence of fluorine bonded nitrogen and appearance of an additional peak at 402.1 eV that corresponds to the graphitic nitrogen indicating molecular functionalization of VC [Lu et al., 2016].

Table 3.1: X-ray photoelectron spectra (XPS) literature reference of C1s, F1s, N1s and O1s.

S. No	B.E. of C 1s (eV)	B.E. of F 1s (eV)	B.E. of N 1s (eV)	B.E. of O 1s (eV)	Reference
1	284.7 (C-C) 285.6 (C-N) 286.5 (C=N) 287.7 (C-O) 288.9 (C-F)	685.8 (semi-ionic C-F) 688.3 (covalent C-F)	398.2 (pyridinic N) 399.3 (pyrrolic N) 400.8 (graphitic N) 402.9 (N-F)	N.A.	[Na et al., 2017]
2	284.6 (284.6) 285.4 (285.4) 286.6 (286.6) 288.9 (C=O/C=N)	684.8 (Ionic C-F) 686.8 (Semi-ionic C-F)	398.2 (Pyridinic N) 400.4 (Pyrrolic N) 401.4 (Graphitic N) 402.7 (Oxidized N)	N.A	[Jiang et al., 2015]
3	284.6 (C-C sp_2/sp_3) 286.2 (C-O) 287.9 (C=O) 289.0 (-COO-) 288.8 (CF_x (x=1,2)) 290.6 (CF_x(x=2,3)) 292.0 (CF_3) 294.0 (CF_3 with CE)	687.7 (Covalent CF_x) 688.6 (Covalent CF_x with CE) 689.6 (Perfluorinated CF bonding) 690.9 (Perfluorinated CF bonding with CE)	N.A.	531.0 (Carbonyl/carboxyl groups) 532.4 (Hydroxyl group) (CF_xO)	[Zhou et al., 2016]
4	284.8 (C=C)	686.2 (Semi-ionic C-F)	398.9 (Pyridinic N)	N.A.	[Huang et al., 2015]

	285.7 (C-O) 287.1 (C-N or C=O) 288.6 (Semi-ionic C-F) 289.5, 291.1, 292.8 (Covalent C-F) 284.8 (C-C/C=C)	688.1 (Covalent C-F)	400.1 (Pyrrolic N) 401.5 (Graphitic N)		
5	286.5 (C-O) 287.2 (C=O) 289 (COOH/C-F) 293.1 ($C-F_2$/$C-F_3$)	685 (F-TEDA) 690 (Fluorinated carbon materials)	N.A.	N.A.	[Liu et al., 2018a]
6	284.8 (C=C) 286.4 (C-O) 285.8 (β carbon $C-CF_2$ bond) 288.8 (semi-ionic C-F bond) 290.0 (Covalent – CF) 290.3 (Covalent – CF_2) 291.8 (Covalent – CF_3)	686.5 (semi-ionic C-F bond) 687.6 (covalent C-F bond)	N.A.	N.A	[An et al., 2016]
7	284.5 (C=C) 285.4 (C-C) 286.4 (C-O) 287.4 (C=O) 289.3 (semi-covalent CF) 290.5 (C-F)	N.A	N.A.	N.A	[Jung et al., 2015]
8	285.7 (C-N) 286.3 (C=N) 289 (O-C=O)	685.6 (semi-ionic C-F)	398.3 (pyridinic N) 399.8 (pyrrolic N) 400.7 (graphitic N)	N.A.	[Zhou et al., 2015b]

9	291.1 (C-F) 284.5 (C=C) 285.4 (C-C) 286.2 (C-O) 287.4 (C-N) 288.6 (semi-ionic C-F)	684.6 (Ionic C-F) 685.6 (Semi-Ionic C-F)	399.5 (C-N) 401.9 (Graphitic N)	531.4 (C=O) 533.1 (C-OH)	This work

NA: Not available

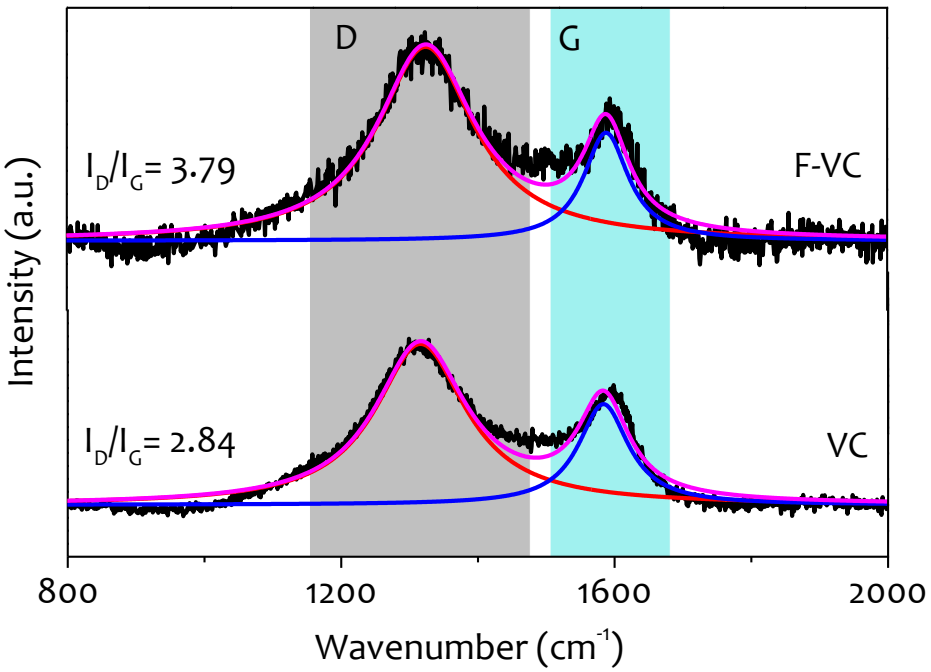

Figure 3.6: Raman spectra of pristine and fluorinated VC.

Raman spectra of VC and F-VC are shown in Figure 3.6. Fluorination of carbon is expected to create disorder and defects in sp^2 hybridized carbon and thus increases the defect density in the graphitic carbon [An et al., 2016]. The signature D-band and G-band of graphitic carbon are observed in the spectrum of both the samples. An unusual shift in the Raman peaks of F-VC compared to VC towards higher wavenumber is observed in the spectrum. This can be associated with functionalization of the graphitic skeleton by fluorine and the F-TEDA moiety [Bulusheva et al., 2014; Lu et al., 2016]. The intensity ratio (I_D/I_G) of corresponding D and G bands is calculated to quantitatively analyze the defects in VC and F-VC. The low signal-to-noise ratio for the samples is due to the amorphous core with ~3-4 nm thin graphitic shell in VC as reflected from the HRTEM and ED pattern of VC (Figure 3.1). Further, the signal noise increases in F-VC compared to VC due to covalent functionalization of graphitic shell and thus suppressing the Raman peak intensities [Nair et al., 2010]. VC shows an I_D/I_G ratio of 2.84 which upon treatment with F-TEDA (F-VC) shows 33.45% (I_D/I_G= 3.79) increase in defect density. This increase in I_D/I_G is significantly high and attributed to surface modification of carbon with fluorine [Mazánek et al., 2015].

3.3.2 Electrochemical Properties of Fluorinated Vulcan Carbon

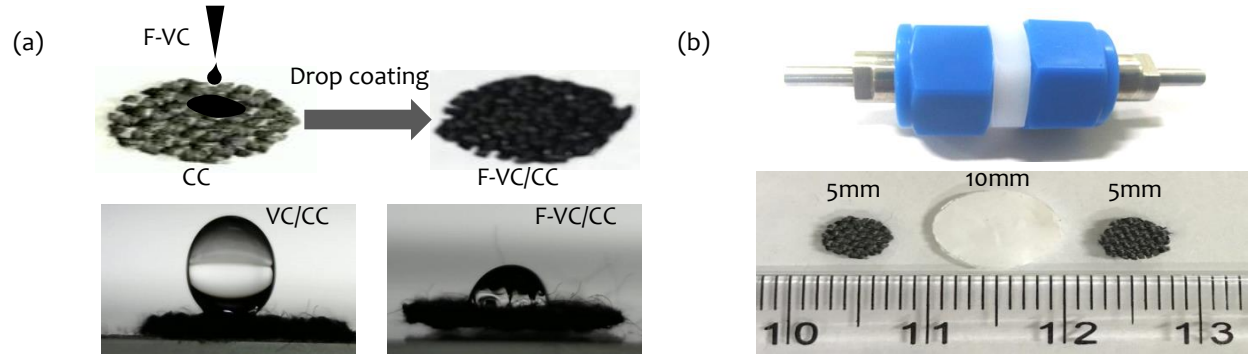

Figure 3.7: (a) Schematic showing the preparation of F-VC/CC electrodes and corresponding surface contact angle measurement on F-VC/CC and VC/CC modified carbon cloth surface. (b) Swagelok cell assembly of supercapacitor device with the electrode and separator shown at the bottom.

The F-VC/CC electrode is prepared by drop coating F-VC/CC on conducting carbon cloth and air dried for 24 h before use. The surface properties were examined by measuring the contact angle of a 5µL water droplet on the electrode surface. As seen in Figure 3.7a, the F-VC/CC becomes hydrophilic (contact angle: 68.4°) in contrast to VC/CC, which is observed to be hydrophobic with a large contact angle of 136.4°. The dramatic change from hydrophobic VC to hydrophilic F-VC upon fluorination can be related to the covalent modification of carbon matrix with fluorine and organic moiety of F-TEDA during fluorination process. The two electrode supercapacitor devices were made in symmetric configuration in a Swagelok type cell with electrodes VC/CC and F-VC/CC as current collectors, Celgard™ membrane as separator and 3M KOH as electrolyte (Figure 3.7b).

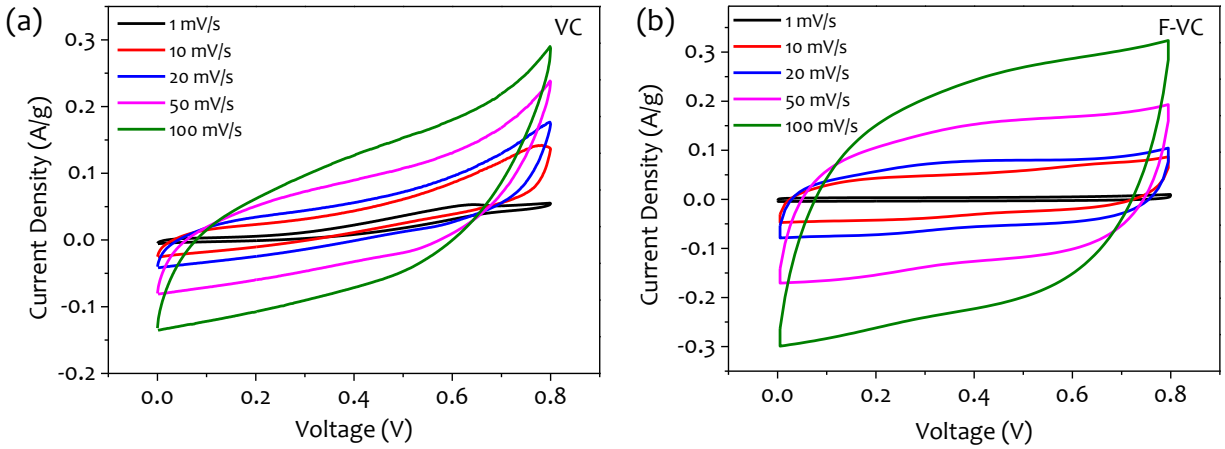

Figure 3.8: Cyclic voltammetry curves at different scan rates for (a) VC/CC and (b) F-VC/CC electrode based devices.

The electrochemical properties of the two electrode devices are analyzed by performing cyclic voltammetry for both VC/CC and F-VC/CC devices at varying scan rates in the potential range of 0-0.8 V. The cyclic voltammogram of VC/CC electrode is leaf-shaped at all scan rates indicating highly resistive nature of the device (Figure 3.8a). However, F-VC/CC device exhibits quasi-rectangular CV curves with the increased size of the loop indicating higher double layer capacitance (Figure 3.8b).

Figure 3.8a shows the comparative CV plots of VC/CC and F-VC/CC devices at a scan rate of 100 mV/s. Clearly, F-VC/CC device shows much better capacitive behaviour in terms of a lower time constant as evident from the shape of the CV curves. Further, F-VC/CC device shows much higher current density in comparison to VC/CC due to the additional charge storage capability incorporated due to the presence of fluorine.

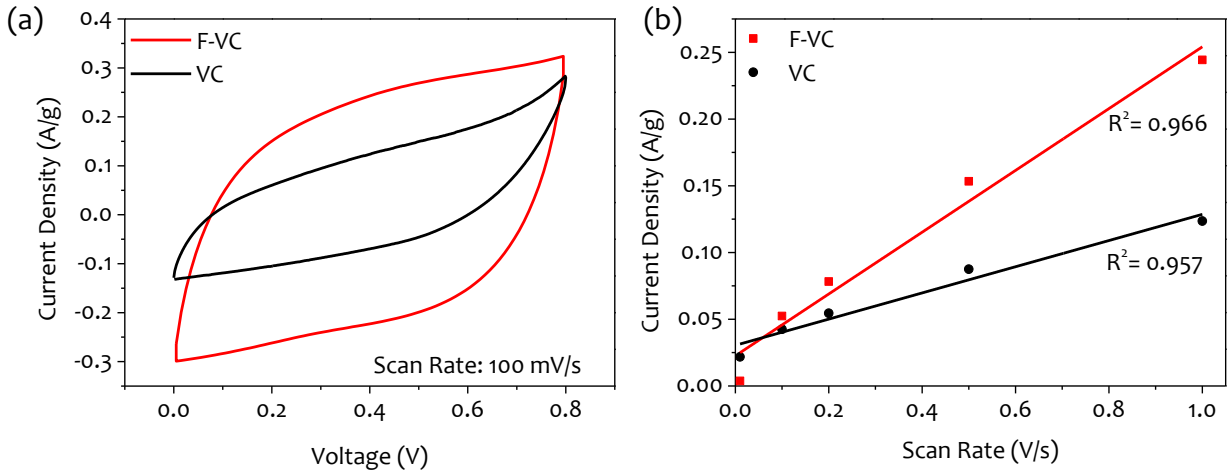

Figure 3.9: (a) Cyclic voltammetry curves of VC/CC and F-VC/CC based devices at scan rates of 100 mV/s and (b) Current density as a function of scan rate and corresponding linear fitting for the data at 0.4V.

There is a significant increase in the specific capacitance values of F-VC/CC with respect to VC/CC at all the scan rates revealing better supercapacitive behaviour. As expected, the current density increases linearly with increasing scan rate for both the devices. The charge and discharge cycle current densities possess a well-fitted linear relationship with the scan rates (R^2 values of 0.966 and 0.957 for F-VC/CC and VC/CC respectively). The linear relation shows that the reaction at the electrode/electrolyte interface is surface controlled for both the electrodes. However, the F-VC/CC exhibits ~3.5 times steeper slope than the VC/CC showing superior supercapacitive behaviour of F-VC/CC electrodes (Figure 3.9b).

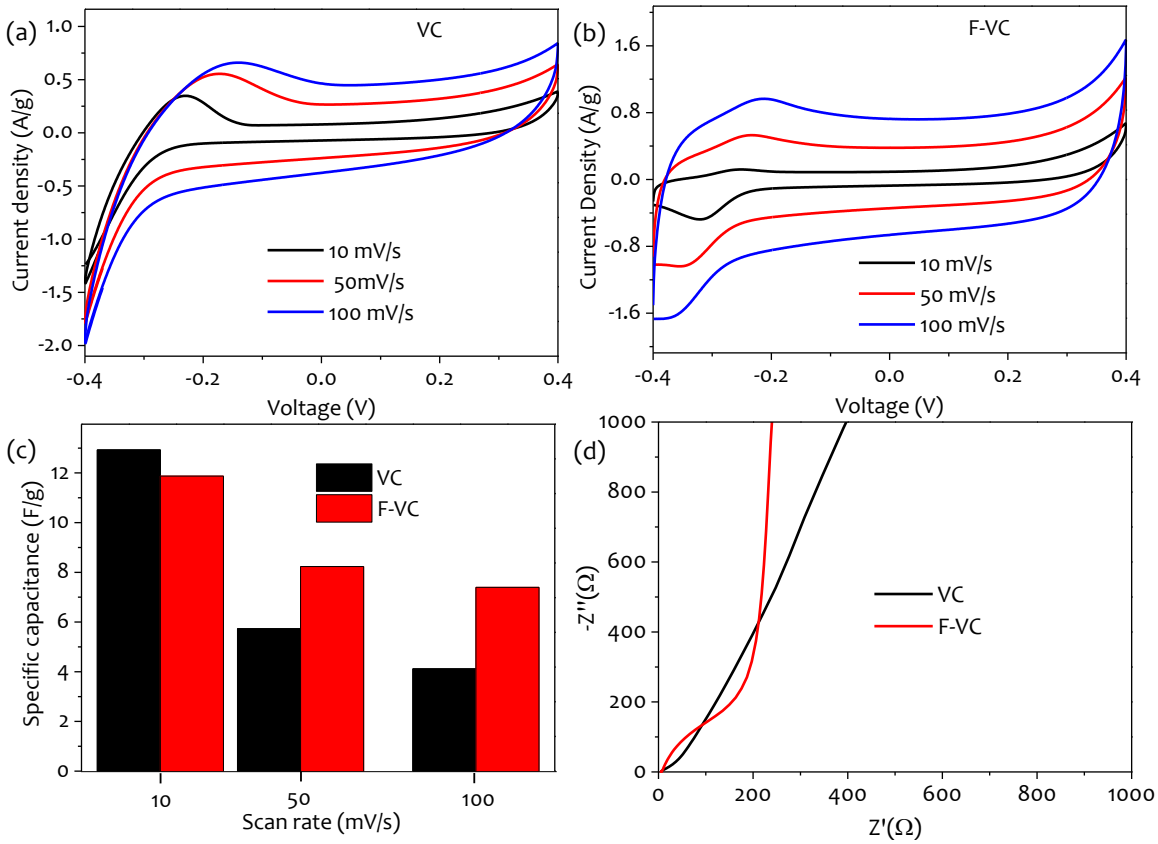

Figure 3.10: Cyclic Voltammetry curves performed in 3-electrode geometry at different scan rates for (a) VC and (b) F-VC. (c) Specific capacitance at different scan rate and (d) Nyquist plot for VC and F-VC in 3-electrode geometry.

The specific capacitance of the supercapacitor reported in two-electrode device is relatively low. However, the electrode possess one order higher specific capacitance (8.23 F/g) as measured from the CV curves of VC and F-VC at different scan rates in 3-electrode geometry (Figure

3.10a,b). A bar graph representation of specific capacitance at different scan rates is shown in Figure 3.10c. Further, the Nyquist plot in three-electrode geometry show reduced charge transfer resistance for F-VC at high frequency region (Figure 3.10d). However, the overall specific capacitance is lower than the other carbon forms due to lower surface area and conductivity of VC (Table 3.2).

Table 3.2: Comparison of BET surface area, conductivity and specific capacitance of common carbon materials.

S.No.	Sample	BET-specific surface area (m^2/g)	Conductivity (S/cm)	Specific Capacitance (F/g)	Reference
1	Vulcan XC-72R powder	238	2.77	5 (@50 mV/s)	[Pérez-Rodríguez et al., 2018]
2	CNT	120-500	10^4-10^5	50-100	[Sur, 2012]
3	Graphene	2630	10^6	100-200	[Sur, 2012]
4	Activated Carbon powder	1000-3500	0.1-1	<200	[Sur, 2012]
5	VC powder (3-electrode)	248	-	5.73(@50 mV/s)	This work
6	F-VC powder (3-electrode)	164	-	8.23 (@50 mV/s)	This work
7	VC device	248	-	0.61 (0.79 mF/cm^2)	This work
8	F-VC device	164	-	6.31 (12.24 mF/cm^2)	This work

3.3.3 Energy Storage Performance of Fluorinated Vulcan Carbon

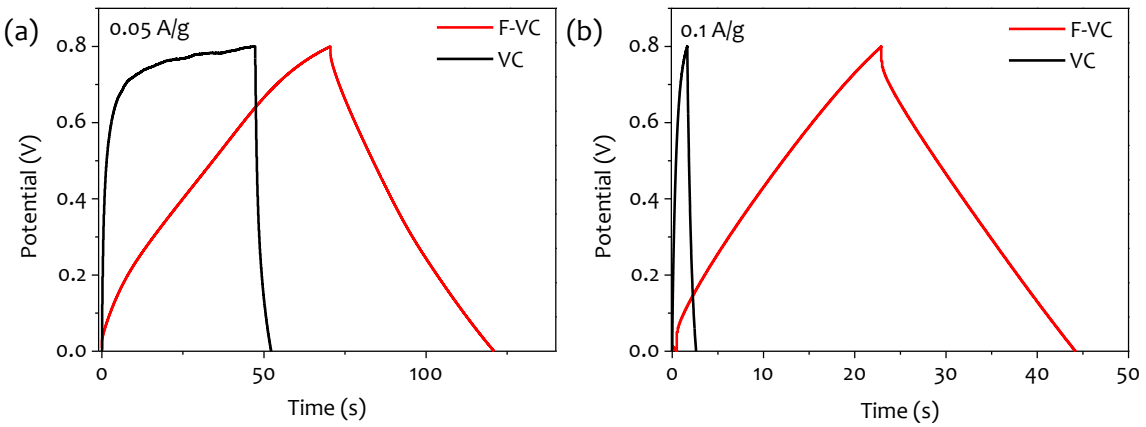

Figure 3.11: Galvanostatic charge-discharge (GCD) curves at current densities of (a) 0.05 A/g (b) 0.1 A/g

Figure 3.11a show the charge-discharge curves at a low current density of 0.05A/g for F-VC/CC and VC/CC electrodes. As seen in the figure, VC/CC shows a very sluggish charging behaviour with a fast discharge profile making it unsuitable for supercapacitor application. This unusual GCD curve can be due to high polarization of the device at low applied current density, which is attributed to the poor quality and hydrophobicity of the carbon material. For this reason, VC is mainly used as a conductive binder material and not as active carbon electrode like other forms of carbon materials. However, it is interesting to note the remarkable improvement in the charge-discharge profile of F-VC/CC electrodes with fluorinated carbon. The GCD curve of F-VC/CC shows symmetric triangular behaviour resembling that of an EDLC supercapacitor. At a

current density of 0.1 A/g, the discharge time for F-VC/CC device increases by more than an order of magnitude in contrast to VC/CC with small IR drop implying superior charge storage capability (Figure 3.11b).

The specific capacitance values calculated from charge-discharge profiles at different current densities ranging from 0.05-0.5 A/g are shown in Figure 3.12. The overall specific capacitance for F-VC/CC electrodes is ~15 times higher than that of VC/CC at all current densities.

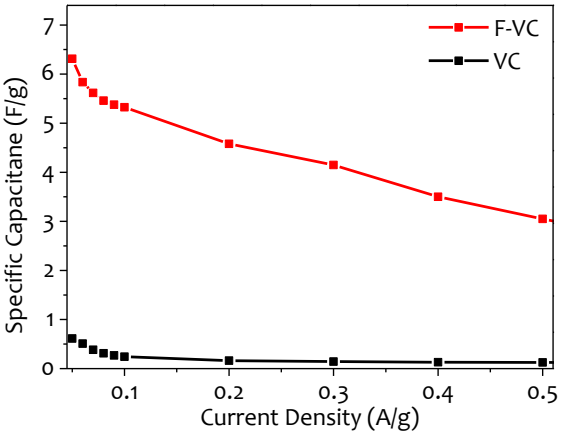

Figure 3.12: Specific capacitance at different discharge current density of VC/CC and F-VC/CC devices.

The specific capacitance of the F-VC/CC and VC/CC based electrodes are calculated to be ~12.25 and ~0.79 mF/cm^2 respectively at a current density of 0.05 A/g. At current densities greater than 0.5 A/g, the performance of F-VC/CC depreciates giving an above limit to the applied current density for charging the device. The overall specific capacitance is low due to concomitant decrease in specific surface area of F-VC on fluorination (Table 3.2). However, it is worthwhile to appreciate the relative increase in the specific capacitance due to an increase in surface polarity induced by semi-ionic C-F bond. Further, fluorination of carbon material has been known to improve charge transfer, decrease resistance and increase energy storage [Li et al., 2016].

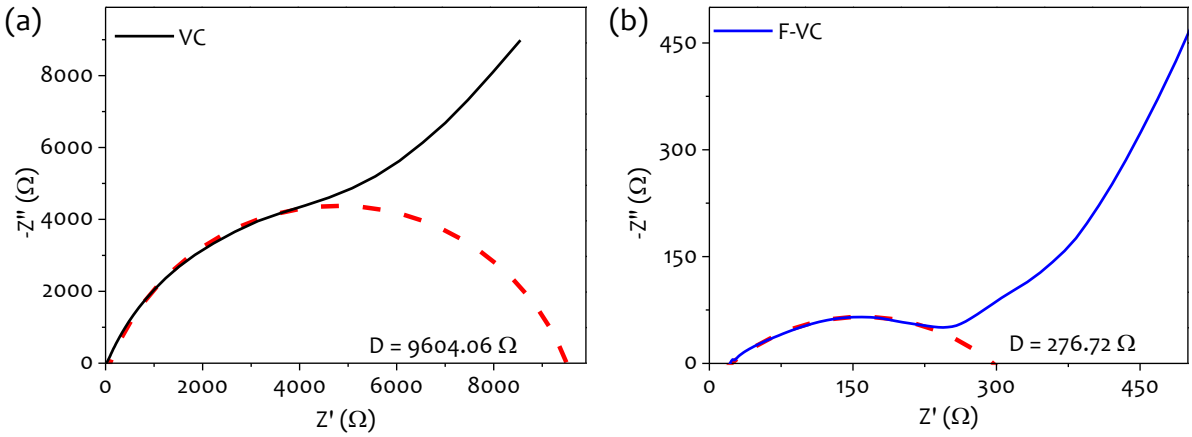

Figure 3.13: Nyquist plots of the fabricated supercapacitors with fitted semicircle of (a) VC/CC (b) F-VC/CC.

To get an understanding about the resistances present in the fabricated devices, electrochemical impedance spectroscopy (EIS) analysis of the VC/CC and F-VC/CC devices is performed in the frequency range of 0.1-10^6 Hz (Figure 3.13a,b). The diameter of the semi-circle in the high frequency region of the Nyquist plot represents the charge-transfer resistance (R_{ct}) at the electrode/electrolyte interface. VC/CC device exhibit a very large diameter (9604.06 Ω) in comparison to the F-VC/CC (276.72 Ω) device indicating a considerable drop in R_{ct} values.
For the practical usage of a device, cyclic stability is one of the critical factors. The stability of F-VC/CC device was analyzed by charging and discharging at a fixed current density of 1 mA/g for 10,000 cycles as shown in Figure 3.14.

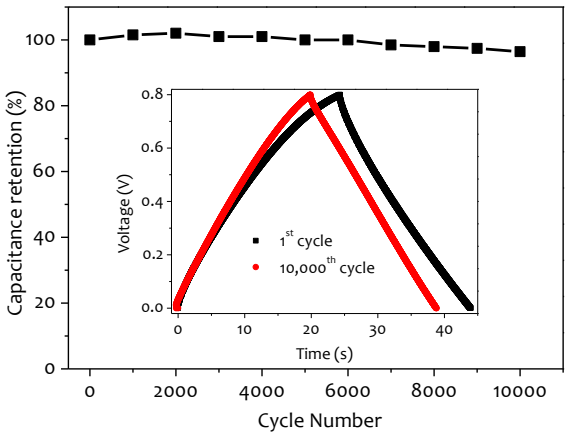

Figure 3.14: Cyclic retention over 10,000 cycles of F-VC/CC based supercapacitor. The inset shows the GCD curve of 1st and 10,000th cycle.

The F-VC/CC based device exhibits capacitance retention of 96.42% even after 10,000 cycles. Figure 3.14 inset shows the GCD curves after 1st and 10,000th cycles. It can be seen that the charging profile of the device improvises after cycling. Further, the capacitance increases after 1st cycle till 2,000th cycle and then decreases gradually at a slow rate. This type of behavior is expected in EDLCs, due to the enhancement in the wettability of the electrodes after initial cycles. Though EDLCs are well-known for excellent cyclic stability, the long-term stability of fluorinated carbon materials has always been a challenge. However, in this study, the observed cyclic stability of fluorinated carbon material (C-F) as electrode material in supercapacitors is noteworthy.

3.3.4 Energy Storage Performance of Fluorinated Nanocarbon from Polymeric Waste

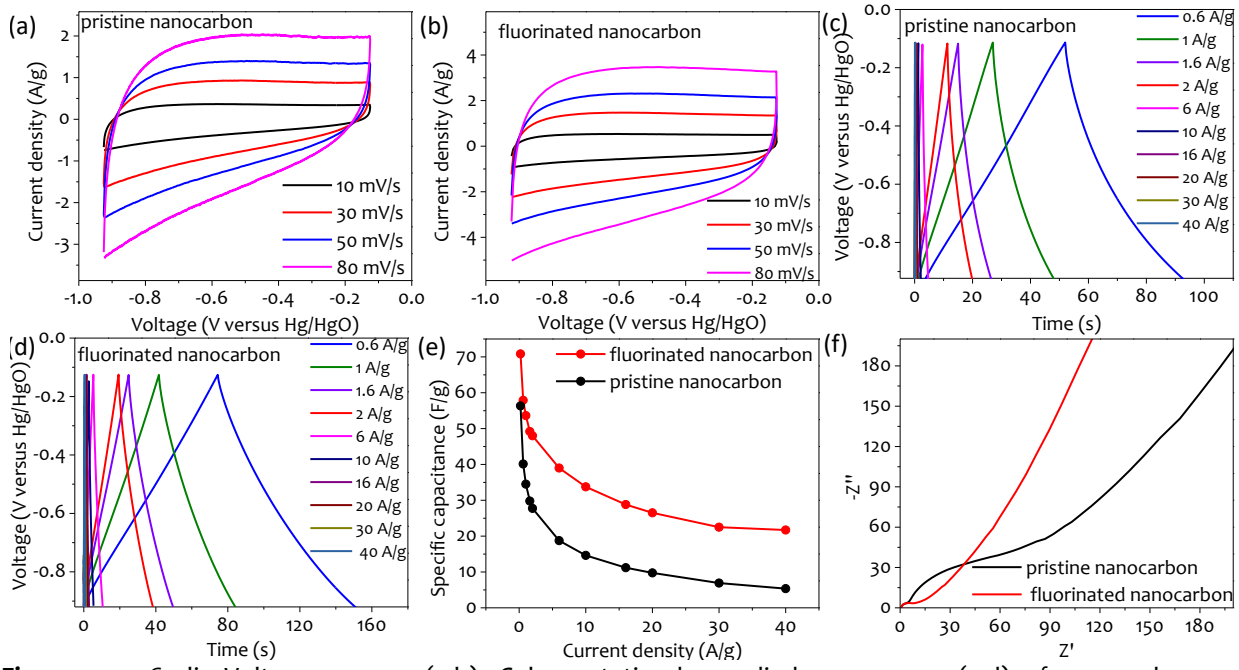

Figure 3.15: Cyclic Voltammograms (a,b), Galvanostatic charge-discharge curves (c,d) of nanocarbon and fluorinated nanocarbon derived from polymer, respectively. Comparative (e) specific capacitance and (f) Nyquist plots for pristine and fluorinated nanocarbon.

Inspired by the enhancement in the specific capacitance of the commercially available carbon (Vulcan carbon) upon fluorination, carbon nanomaterial produced in the laboratory from polymeric waste was fluorinated by the developed methodology. The electrochemical performance of the pristine nanocarbon and fluorinated nanocarbon from polymeric waste in three-electrode geometry is shown in Figure 3.15. As expected, pristine nanocarbon shows a leaf-like CV response (Figure 3.15a) at different scan rates, while fluorinated nanocarbon

exhibits a quasi-rectangular response with higher current values (Figure 3.15b). Similarly, the GCD response of pristine nanocarbon shows a quasi-triangular response (Figure 3.15c), which upon fluorination, exhibits a symmetrical triangular response (Figure 3.15d) at a wide current density range of 0.6-40 A/g. The specific capacitance calculated from the GCD response is shown in Figure 3.15e. Fluorinated nanocarbon exhibits a specific capacitance of 70 F/g (at 0.6A/g) and 21.7 F/g (A/g), which is 25% and 300% higher than that of pristine nanocarbon respectively. Further, charge-transfer resistance (R_{ct}) at the electrode/electrolyte interface in fluorinated nanocarbon shows a large diameter in comparison to flurintated nanocarbon, indicating a considerable drop in R_{ct} values (Figure 3.15f). Hence, this fluorination approach results in carbon nanomaterial with enhanced capacitive behavior due to the collective effect of improved charge-transfer ability, enhanced charge storage, cycling stability, and wettability of the carbon electrodes.

3.4 Conclusions

In conclusion, fluorination of commercially available low-cost graphitic carbon is carried out using an electrophilic fluorinating precursor, F-TEDA (Selectfluor™), via a simple-solution process at a low temperature of 70 ^{o}C and annealing at 150 ^{o}C. The fluorinated Vulcan Carbon coated on carbon cloth used as electrodes in a two-electrode supercapacitor device exhibits one order higher specific capacitance in comparison to pristine Vulcan Carbon device. The fabricated device shows excellent capacitance retention over 10,000 cycles. The fluorine atom introduced into the carbon lattice endows enhanced charge mobility, surface wettability, cycling stability, and decreased charge transfer resistance. This method is extendable to various types of carbon for the fabrication of electrodes for supercapacitors and other energy devices with high electrochemical performances. It further opens up the door for various applications that require fluorine functionalized carbon material for better performance.